2

Confocal Scanning Laser Microscopy: Applications for Imaging Dynamic Processes in Skin *In Vivo*

Melissa Chu[1], Nikiforos Kollias[1] and Michael A. Luedtke[2]
[1]Johnson & Johnson Consumer Companies, Inc.
[2]Codman & Shurtleff, Inc.
USA

1. Introduction

In vivo confocal scanning laser microscopy (CSLM) is a powerful imaging technique that enables physicians and researchers to evaluate skin dynamically and non-invasively at the cellular level. Traditionally, biopsy and histological processing are required to study the cellular details of skin. This involves tissue excision and staining, which may introduce artifacts to the sample. Staining and immunostaining have been used to identify specific proteins and organelles successfully. With CSLM, the examined areas are not damaged, removed, or processed, so imaging can be performed as often as desired. Studying dynamic changes in skin over an extended period of time or as a response to treatment is feasible. Unlike the vertical sections obtained by routine histology, *en face* (horizontal) images are captured with CSLM. During the last 20 years, advances in technology have resulted in images that are now near histological resolution and have enough detail for histological analysis (Pellacani et al., 2008; Scope et al., 2007; Rajadhyaksha et al., 1999).

CSLM has been used in dermatology to assess skin lesions and skin conditions without biopsy. Both benign and malignant melanocytic skin tumors have been described and diagnosed, and proliferative and inflammatory skin diseases have been characterized (Gonzalez & Gilaberte-Calzada, 2008; Calzavara-Pinton et al., 2008). Margins of lesions are also identifiable from non-lesional skin. For physicians, CSLM provides real-time diagnostics and the chance to follow the evolution of skin lesions over time, which would not be feasible otherwise.

Whereas the majority of CSLM skin research concentrates on dermatological conditions, this chapter focuses on capturing and studying non-diseased tissue, both healthy and wounded human tissue. We first assess the effect that the incident laser wavelength has on the images captured by comparing CSLM systems of three different wavelengths. Then, we specifically discuss two studies in which we use CSLM to study skin morphology and physiology: 1) a comparison of infant and adult skin morphology and 2) the wound healing response of micro-injuries in otherwise healthy human skin. The micro-injury study focuses on dynamic responses in skin over time. Ethically we are committed to minimize biopsy collection when studying healthy human skin. CSLM is our sole alternative to studying skin morphology and physiology at the cellular level non-

invasively and to monitor biological processes such as blood flow at video rate, with the added benefit of investigating skin *in vivo*.

2. Structure of skin

2.1 Skin morphology

The skin is composed of two layers, the epidermis and dermis. The epidermis is the outermost layer of the skin. The top layer of the epidermis is known as the stratum corneum and functions as the barrier to the outside world. Its consists of corneocytes, or dead keratinocytes, which contain primarily keratin. Corneocytes are approximately 1 μm thick and 1000 μm^2 in area. The stratum corneum, approximately 10-15 μm thick, encounters various insults from the outside world, such as UV radiation, friction, scrapes and cuts, and irritants.

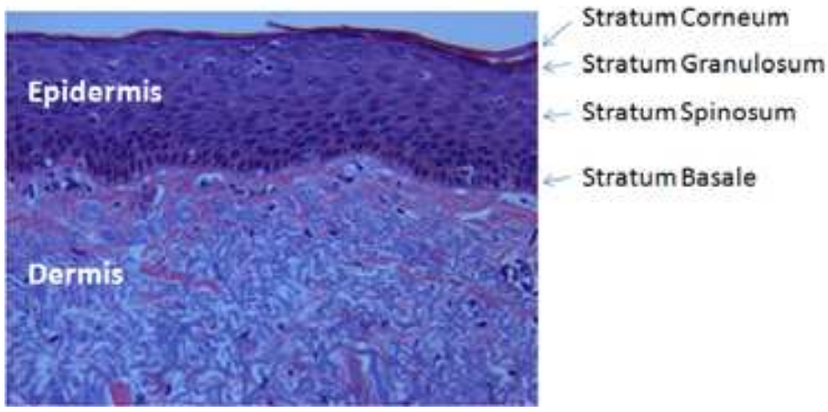

Fig. 1. Various layers of skin are noted in this histology slide of human skin. (hematoxylin and eosin stain, 20x)

Below the stratum corneum is the viable epidermis. The viable epidermis is composed of living skin cells, or keratinocytes, and is 50-100 μm thick. There are various layers noted within the epidermis: stratum granulosum (granular layer), stratum spinosum, and stratum basale. The stratum basale is a single layer of cells resting on the basal membrane that includes both keratinocytes and melanocytes. Keratinocytes are generated by mitosis in the stratum basale, and the cells differentiate and increase in size as they progress to the uppermost layer of living cells. At the highest layer, they then stop functioning as cells and exist as dead cell envelopes that compose the stratum corneum, which will eventually be shed. Melanin, pigment that contributes to the color of skin, is produced by melanocytes and is distributed to keratinocytes. The dermal-epidermal junction, where the epidermis meets the dermis, often consists of dermal papillae, which are small finger-like protrusions of the dermis into the epidermis. The dermis (1-3 mm) contains connective tissue, vasculature, and various appendages. The connective tissue, primarily collagen and elastin, provides cushion and elasticity to the skin. Blood and lymphatic vessels confined to the dermis bring nutrients to and remove waste from the keratinocytes.

2.2 Endogenous skin chromophores

Skin has different endogenous chromophores that have unique physical characteristics. Aside from optical scatterers found within skin, there are absorbers and fluorescent

chromophores as well. In fluorescence, a particular stimulus at a given excitation wavelength elicits an emission at a higher wavelength due to the Stokes shift and basic principles of fluorescence. If coherent light of a specific wavelength is used in conjunction with appropriate filters and a detector sensitive enough to measure the fluorescence signal, endogenous (and exogenous) chromophores can be measured quantitatively from the skin surface.

In summary, skin is a complex organ with different appendages and structures that can scatter and absorb light. Table 1 lists some of these endogenous chromophores found within skin (Kollias, 1995).

Endogenous Skin Chromophore	Characteristic	Principle wavelength (nm)
Melanin	absorber and scatterer	Monotonic increase from 700-300 nm
Collagen crosslinks	fluorescent	X335 M380; X370 M460
Elastin crosslinks	fluorescent	X420 M500; X460 M540
Oxy Hemoglobin	absorber	412, 542, 577
Deoxy Hemoglobin	absorber	430, 555, 760

Table 1. Different endogenous chromophores within skin at wavelengths of interest. Excitation (X) and Emission (M) wavelengths are provided (Kollias, 1995).

3. Theory and technique of CSLM

3.1 Principles of CSLM

The confocal microscope is elementally comprised of a coherent scanning laser light source, condenser lens, objective lens, and detector. Details involving the intricacies of the optics, point spread function and other tissue-light interactions (Webb, 1996; Webb, 1999) are not included in this chapter.

A laser light point source illuminates a small region within the skin and is scanned across the skin. Light reflected from this focal point propagates back to the detector through a pinhole aperture after a single collision within the tissue, allowing us to observe reflections from single scattering events. Light from the in-focus plane is collected, as light emanating from above and below the focus plane minimally passes through the pinhole to the detector, resulting in images of high resolution and contrast. The term "confocal" stems from this design in which the pinhole in front of the light source and the pinhole in front of the detector are in optically conjugate focal planes. Figure 2 illustrates the principle of confocal microscopy.

For the research discussed in this chapter, a commercial *in vivo* confocal scanning laser microscope (Vivascope 1500, Lucid Inc., Rochester, NY) was used to non-invasively study skin at the cellular level. Unless otherwise stated, a 785 nm wavelength laser was used in the microscope.

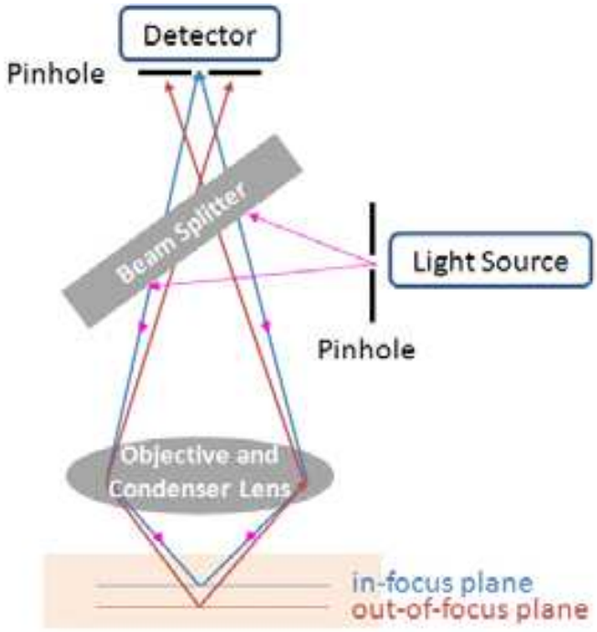

Fig. 2. Principle of CSLM. Note the same optical path is used for the detector and the source. Optics are used to direct the light towards the detector.

3.2 Image acquisition

To minimize lateral movement of the skin and motion artifacts, a metal tissue ring is adhered to the skin with a double-sided adhesive acrylic tissue window. The tissue ring, which holds the optical coupling (ultrasound gel), is magnetically attached to the microscope housing of this device.

Once the optical paths are fixed relative to the tissue imaged, a point source is rastered quickly within a conjugate focal plane. The pinholes are then used to reduce the amount of light that generates an image on the photodetector. This detector then produces the images as they are seen on screen.

There are various methods of generating a scanning laser effect (Webb, 1999). For example, a Nipkow disk (sometimes known as Nipkov disk) is a disk with a series of holes in it that spins rapidly. While resolution along a scanline is very high, scan rates are limited to the number of holes found within the disk. The images generated with these types of disks can cause a flickering and result in a less than video sampling rate.

Commercially available *in vivo* CSLM equipment typically uses a laser light point source that is scanned in a raster pattern by a multi-faceted polygon mirror and an oscillating galvanometric mirror. The polygon mirror rotates at a high speed, a few hundred revolutions per second, while the galvanometer oscillates at a slower speed and is driven by a saw tooth signal. The beam scans left to right along the horizontal axis, and after a single horizontal scan, the beam quickly returns to the starting point and shifts along the vertical axis to begin a new scan. Each horizontal scan line is generated by each facet of the quickly rotating multi-faceted polygonal mirror, and the vertical shift occurs during the oscillations of the galvanometer. Scanning is performed at a rate of 9 frames per second, and the resulting (1000 pixel x 1000 pixel) image is equivalent to an *en face* 0.5 mm x 0.5 mm horizontal microscopic section, at closer to full motion and flicker-free video rates.

The microscope can capture a series of focal planes at different depths by changing the focal length of the beam, and it has the capability of imaging 200-300 µm below the skin surface. A series of images is typically captured from the top of the stratum corneum (SC), through the epidermis and papillary dermis, and down into the superficial reticular dermis, forming a vertical image stack. This is known as "optical sectioning".

3.3 Visualization of cellular structures

Each two dimensional optical section is 500 µm x 500 µm in size and is obtained in grayscale relative to the positioning of the surface of the skin. Structures within tissue are visualized based on their optical properties, changes of index of refraction, and absorption within the tissue. There is good contrast within living tissue, allowing microscopic structures and cellular details in the epidermis and superficial dermis to be visualized. Contrast in images is provided by differences in refractive index of organelles and microstructures, such as keratin, melanin, and collagen, compared to the background. Melanin has one of the largest index of refraction found in skin, which makes it one of the strongest contrast agents in skin, and results in greater backscattering of light, causing pigmented structures to appear bright (Rajadhyaksha et al., 1995). Other structures such as inflammatory infiltrates, dendritic cells, and capillaries can also be imaged with CSLM. Total light is reflected back when structures appear white, while no reflection is represented by black.

3.4 Quantitative analysis

Both qualitative and quantitative analyses can be performed on the acquired CSLM images. From individual images, cellular size can be measured. The thickness of the SC and epidermis can also be measured when analyzing images captured from the image stacks. From the 8-bit grayscale image, changes of intensity can be normalized to the laser power for quantitative analysis of tissue structure within the images. This technique of quantifying a region of interest (ROI) or group of pixels found within an image is a powerful technique to measure changes in skin microstructure non-invasively and semi-automatically. With the appropriate software analysis routines, gigabytes of image data can be analyzed and meaningful measures can be made on data that was previously too cumbersome to analyze.

3.5 Imaging limitations

While CSLM is optimal for imaging optically thin tissues, certain appendages and other optically thick samples limit its capabilities. Since the microscope is a fluid immersion microscope, certain skin appendages and structures could change morphology while immersed in fluid. Bubbles, improperly adhered and inconsistent placement of the tissue ring are challenges that plague this imaging modality and increase the complexity of acquiring quality images. Due to the high magnification, the images acquired are prone to subject movement. Since *in vivo* CSLM measurements are made on living subjects who breathe, have a moving circulatory system and have involuntary movements, there will occasionally be added "noise" or movement in the acquired images. Great attention should be paid to acquiring quality images prior to arriving at conclusions. When imaging the same area over time, locating fiducial marks within tissue structures or carefully demarking the surface area is critical to finding the same cellular structures and to detect changes over time. Despite these various limitations, CSLM is one of the only methods to non-invasively image cellular morphology and is an extremely powerful tool if used correctly.

4. Incident wavelength effects on CSLM imaging

An important factor when imaging the skin with CSLM is to understand the effect that the incident light wavelength has on the images captured. Recognizing the various effects that the incident wavelength has on the images will help to properly understand and resolve different biological structures within skin. Near-infrared wavelengths are typically chosen for *in vivo* CSLM skin imaging because they can penetrate deeply into the skin. Shorter wavelengths and smaller pinholes can increase the axial and lateral resolution of reflectance imaging. The disadvantage of shorter incident wavelengths is shallower penetration depths, which may be attributed to the wavelength dependence of light scattering and absorption of light by endogenous skin tissue chromophores.

A study was performed to investigate the effect of three different wavelengths of incident light when imaging with CSLM: 405, 785, and 830 nm (Luedtke et al., 2009). These incident wavelengths were chosen because 1) 830 nm is the standard incident wavelength for commercial *in vivo* CSLM systems and is presumed to have the best penetration depth; 2) 785 nm could excite fluorescent dyes, e.g., indocyanine green, while also having good penetration depth; and 3) 405 nm could excite autofluorescence in skin and provide improved resolution in reflectance measurements, due to the shorter wavelength. Optical phantoms and human skin were imaged with these three incident wavelengths.

To determine differences attributed solely to the incident wavelength, the optics of the systems were made as comparable as possible. The optical design, incident laser wavelength, optical coatings and detectors are some of the factors that need to be considered. For the study, three microscopes were used: the commercially available Vivascope 1500 which uses an 830 nm laser, and two custom Vivascope 1500 microscopes (Lucid, Inc., Rochester, NY) to allow imaging with 405 nm and 785 nm lasers. The 785 nm and 830 nm CSLM systems were identical with regard to specifications. The exact same objectives were used for both microscopes, with the only major difference being the incident light source, to eliminate artifacts that may occur due to a change in optics. The 405 nm CSLM was designed to be comparable to the 830 nm system. Some adjustments were required to maintain a relative similarity despite the large wavelength difference, specifically changes in polygon mirror coatings, antireflective coatings on the telescope optics and objectives, pinhole size, and detector. These changes were essential to maintain equivalent optics, while delivering reflectance images that could be compared across the microscopes.

CSLM System	Polygon Mirror Coating	Telescope Design	Pinhole Diameter	Detector
785 and 830 nm systems	Lincoln Laser 01 protected gold	Optimized for 750-1400 nm	100 µm	Hamamatsu Avalanche Photodiode (C5460 Series) (Hamamatsu, Japan)
405 nm system	Lincoln Laser 04 enhanced aluminum	Optimized for 406-658 nm	50 µm	Hamamatsu Photomultiplier Tube (R7400U Series) (Hamamatsu, Japan)

Table 2. Differences in design of CSLM systems

In the tissue phantom study, an optical phantom that simulated the optical properties of human skin was evaluated to measure changes due to incident wavelength in a standard

frame of reference. The phantom was comprised of silicone, india ink, and titanium dioxide (Beckman Laser Institute, University of California – Irvine) and had absorption and scattering coefficients of μ_a= 0.08/mm and μ_s=2.53/mm at 600 nm. A 1 mm diameter steel wire was inserted into the phantom so that imaging at the same exact location was feasible. Six replicate image stacks were captured with each microscope, beginning at the surface of the phantom and progressing into the phantom until structures were no longer visible.
The normalized intensity profiles generated for each wavelength microscope show that the three wavelengths have similar rates of exponential decay down to depths of 175 µm (Figure 3). There are surface intensity differences, which may be due to sensitivity differences in the photodetector to each wavelength, or to possible fluorescence in the silicone phantom when excited at 405 nm. The high signal intensity observed in the 405 nm system may also be due to its photomultiplier tube (PMT) photodetector compared to the avalanche photodiode (APD) found in the near infrared wavelength systems.

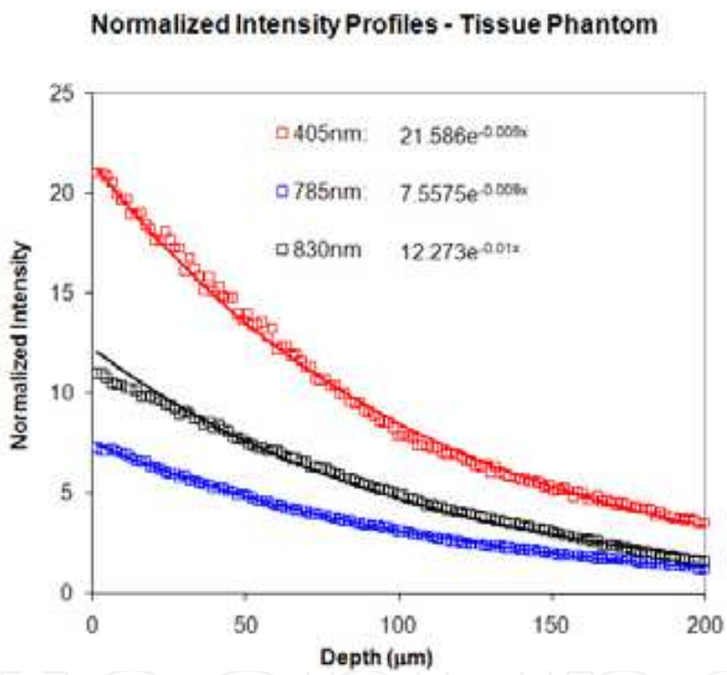

Fig. 3. Normalized intensity profiles of the tissue phantom, from different incident wavelength CSLM systems (405 nm, 785 nm, 830 nm). Normalized intensity refers to normalization of image intensity of a region of interest to the laser power used to capture the image.

In the human study, 8 female subjects, ages 25-45 years old, were evaluated on the upper volar arm after informed consent was obtained. After the tissue ring was applied on the arm, imaging with the three microscopes was performed, without removing the tissue ring. This helped minimize any artifacts that may be introduced when changing tissue windows or placing the tissue ring multiple times on the same site. The order in which microscopes were used was randomized for each subject. To image the same exact site, special attention was paid to identify fiducial marks (e.g., hair follicles and pigmented spots) in surface images to ensure imaging of exact locations. Image stacks were captured at 1.5 µm increments, until structures were no longer visible. For each subject, three image stacks were

acquired at different locations with each microscope. When analyzing these images, the ROIs excluded areas of high contrast, e.g., hair follicles and surface microglyphics. When the three image stacks captured at the same site but with the different wavelength systems were analyzed, the size and shape of the regions were identical, and the average intensity of the ROI was normalized to the laser power used to capture the image (Figure 4).

Imaging with the 405 nm CSLM system was halted after 166 µm because structures were no longer visible due to the weak signal. The laser power of the 405 nm system cannot be greatly increased for better imaging in depth because of the strong absorption by melanin, which results in a stinging sensation for some subjects. Very little light penetration was expected, so imaging to a depth of 166 µm was unexpected. Due to strong endogenous skin tissue chromophore absorbers and increased scattering function, only the upper epidermal features were expected to be seen, but the entire epidermis and part of the superficial dermis were visible when using the 405 nm system. Two possible explanations for this surprising result are 1) the inhomogeneity of skin which may allow light to penetrate deeper than theorized or 2) the papillary dermal collagen reflectance observed in the images.

The intensity profiles were fit to exponential functions using least squares fitting. Data from the 405 nm system can be represented by a one-term exponential function, while data from the 785 and 830 nm systems require two-term exponential functions. When comparing the intensity profiles generated from the optical phantom and human skin, the complexity of the signals from human skin indicate inhomogeneities in skin structure.

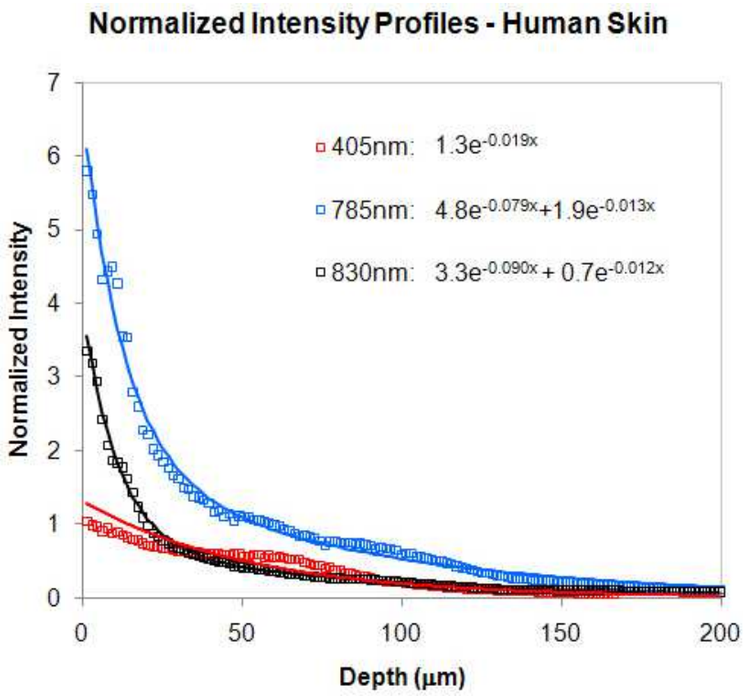

Fig. 4. Normalized intensity profiles of human skin, from different incident wavelength CSLM systems (405 nm, 785 nm, 830 nm)

The choice of wavelength may affect the ability of CSLM to visualize certain skin features, as differences in human skin intensity profiles at each wavelength are observed. The intensity profile generated by the 405 nm system shows an increase in signal intensity near 50 µm,

which corresponds to the presence of dermal papillae near the dermal-epidermal junction. Although the dermal papillae are visible in the 785 and 830 nm images, they are most evident in the 405 nm images, which may indicate that using a 405 nm incident wavelength laser may be best when studying dermal papillae. There is a significant decrease in signal intensity from the 405 nm system, compared to the near-infrared wavelength systems, which is likely due to the absorption of light by collagen cross-links in the superficial dermis. The absorption is significantly reduced at near-infrared wavelengths, leading to strong signal intensities from the 785 and 830 nm systems, making them much better options when studying the superficial dermal tissue.

While the 405 nm system would theoretically generate images with improved resolution, it was not fully realized in this study. This may be due to using a 50 µm diameter pinhole, which may be too large, allowing light from adjacent layers to pass through. Imaging with a 35 µm diameter pinhole shows significantly improved resolution of cellular details.

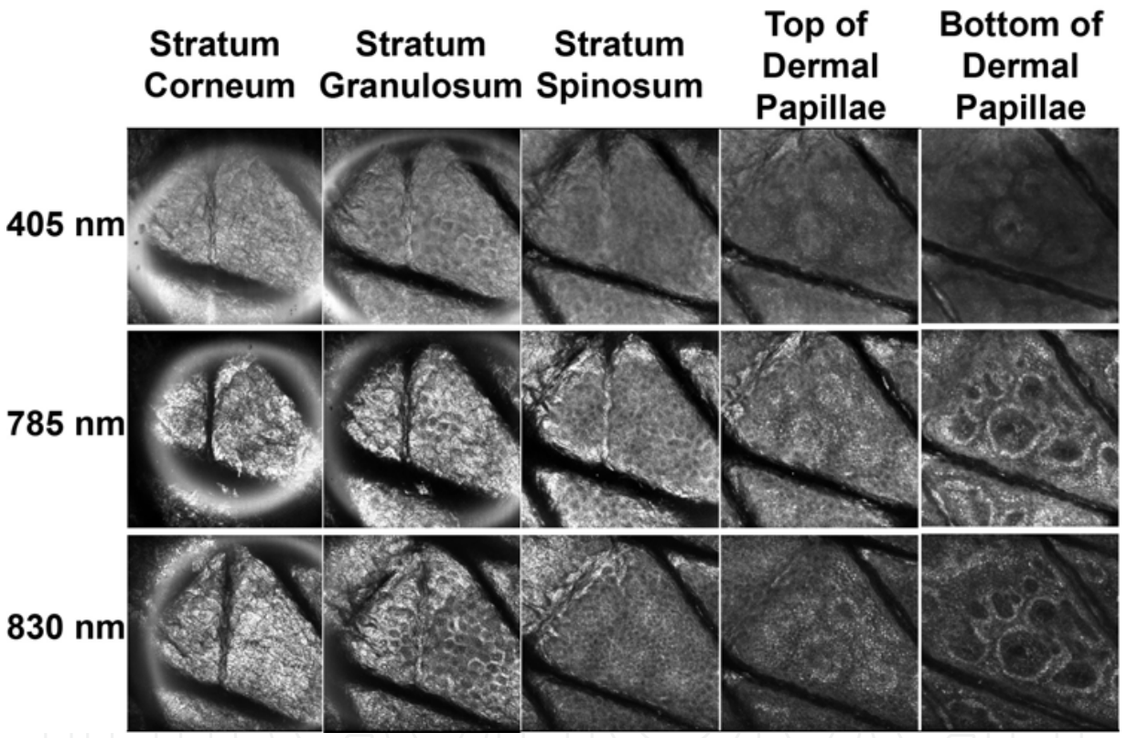

Fig. 5. Differences in image quality are observed with different incident wavelength lasers

It was anticipated that images obtained from the 785 and 830 nm systems would be nearly identical due to the small difference in wavelengths and the absence of skin chromophores that would absorb selectively at either 785 or 830 nm. The intensity values of skin at 785 nm, however, were consistently greater than those obtained at 830 nm. Enhanced contrast was also observed with the 785 nm, allowing better visualization of structures. Despite all efforts to create the microscope setups with nearly identical optics, differences in image detail were revealed at these wavelengths.

Overall, imaging at different wavelengths with CSLM systems can reveal different structural details in cells. Both qualitative and quantitative differences were observed when imaging the same location in healthy human skin with different incident wavelengths. The

405 nm CSLM system provides better spatial resolution than near-infrared wavelength systems, while still penetrating relatively deep into the skin, up to 166 µm. Despite the close proximity of wavelengths, the 785 and 830 nm CSLM systems show differences in signal intensity and structural contrast apparent in images. Optimization of the incident wavelength may improve CSLM performance depending on the application.

5. Comparison of infant and mother skin

Examples of such quantitative analyses of cell size, SC and epidermal thickness, and normalized intensities were used to measure age-related changes in a population of mothers and their biological infants (Stamatas et al., 2009). CSLM allows non-invasive visualization of different functional and microstructure differences between infant and adult skin.
In a clinical study comprised of 20 healthy mothers (25-43 years old) and their biological children (3-24 months old), the skin microstructure of the lower thigh area of infants and adults were examined and compared. Image stacks consisting of at least 32 images were acquired, with an axial section of 1.5 µm in step size. The lower thigh area was examined for ease of measuring infants, as it is difficult to keep them voluntarily still. The mothers held the infants in their laps throughout imaging. Although there was still some movement in the image stacks, every effort was taken to prevent movement of subjects during imaging. SC and epidermal thickness, as well as size of cells in the granular layer, were assessed from the confocal images. Sample images from various image depths are shown in Figure 6, comparing infant and mother skin.

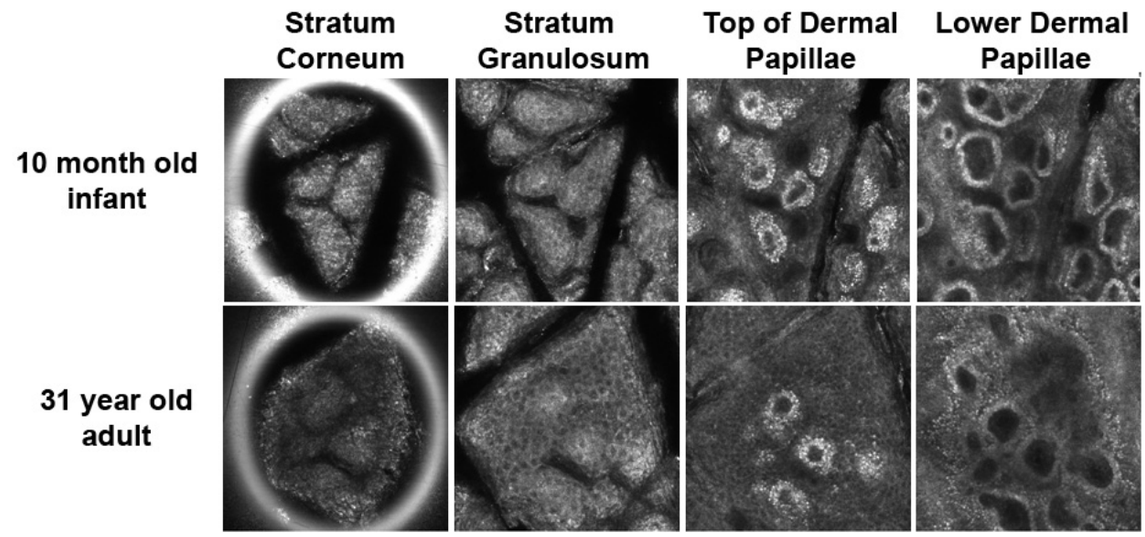

Fig. 6. CSLM images at various depths from sample image stacks of an infant and an adult. Both subjects are African-American. Pigmented keratinocytes are visible surrounding the dermal papillae.

Surface features evaluated showed differences in microglyphic density and surface area. Microglyphics appear as dark lines that separate “islands” of cells in CSLM images. For infant skin, a greater density of microglyphics is present. Differences in epidermal thickness and cell size were also documented. Infant SC and epidermis were found to be 30% and 20% thinner, respectively, than adult SC and epidermis. Infant corneocytes and granular cells

were found to be 20% and 10% smaller, respectively, than adult cells indicating a more rapid cell turnover in infants (Figure 7).

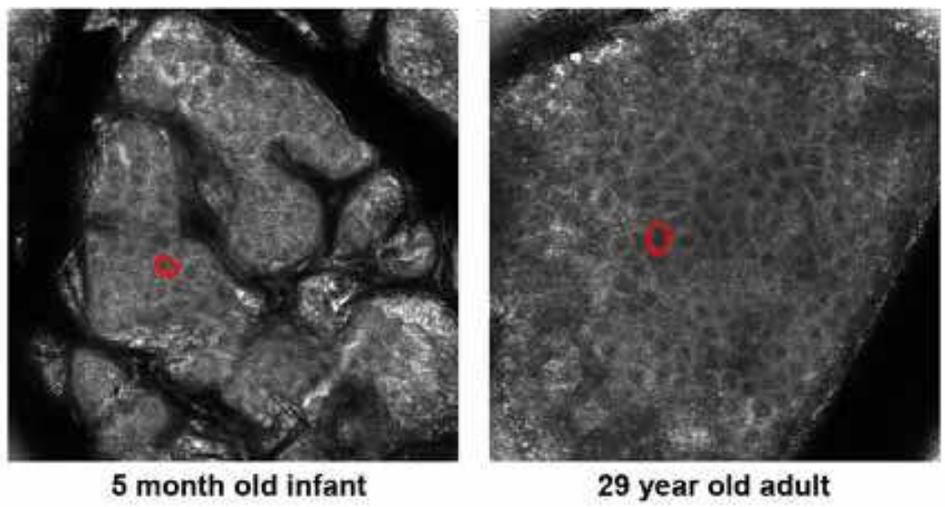

Fig. 7. A granular cell is outlined in infant and adult images.

Dermal papillae density and size distribution also differed. In infant skin, a distinct direct structural relationship between the SC morphology and dermal papillae was observed. A change in reflected signal intensity at ~100 µm, indicating the transition between papillary and reticular dermis, was evident only in adult skin (Figure 8). Upon performing software analysis of the optical sections, a normalized profile as a function of depth was captured.

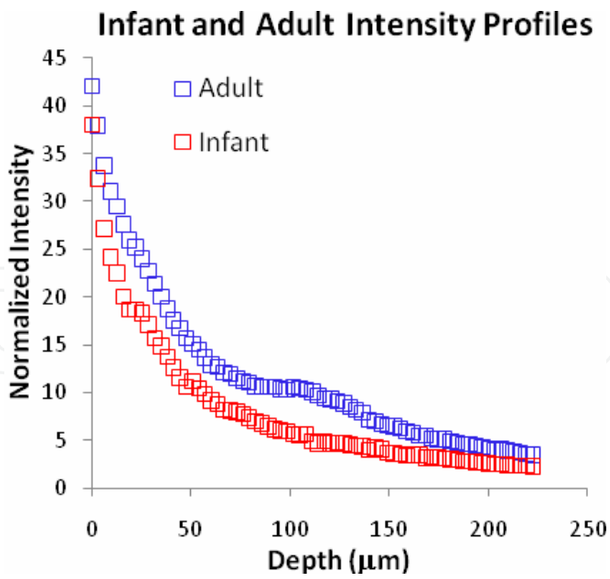

Fig. 8. Normalized intensity profiles as a function of depth, for infant and adult skin.

The centers of the images were analyzed to further account for movement within the images, and the averages were taken within the defined ROI. The ROI was averaged across the optical sections and the triplicate vertical image stacks acquired. These differences in

skin microstructure may help explain some of the reported functional differences and assumptions made regarding skin softness and other aging related effects.

6. Wound healing response of micro-injuries

A common treatment for skin aging is the use of a laser device with infrared wavelength to induce an array of microscopic wounds in the skin. Micro-wounds are created when aqueous components within skin tissue absorb the light, and defined areas of photocoagulation stimulate a wound-healing response in the dermis, resulting in increased production of new collagen and improved skin tone and texture (Hantash & Mahmood, 2007; Manstein et al., 2004; Tannous, 2007). These micro-injuries quickly re-epithelialize by the surrounding undamaged tissue, and CSLM can be used to better understand the dynamic wound healing process as a response to micro-injuries by monitoring them non-invasively (Liu et al., 2009).

A single line of micro-injuries, 1 cm long with approximately 400 μm between centers of micro-injuries, were created with a fluence rate of 60 mJ on the volar forearms of 8 healthy subjects (Fitzpatrick skin type II-VI, ages 27-57 years old). Informed consent was obtained from all subjects. Micro-injuries were evaluated with both CSLM and video microscopy (Hirox, Japan) at various time points to study both short- and long-term effects of treatment (30 minutes, 2, 4, and 21 days post-treatment). Cross-polarized images were captured with video microscopy to highlight sub-surface features, including pigmentation and vasculature. For CSLM imaging, a series of 128 images were acquired, with an axial section of 1.5 μm in step size. To quantify the wound healing process at the microscopic level, the depth-dependent intensity profile from a defined ROI was obtained by calculating the average intensity within the ROI at each depth.

The micro-wounds appear as a line of dark brown spots in the video microscopy image, while they appear very bright in the corresponding CSLM image, captured approximately 80 μm below the SC surface, indicating strong scattering in the micro-wound area (Figure 9).

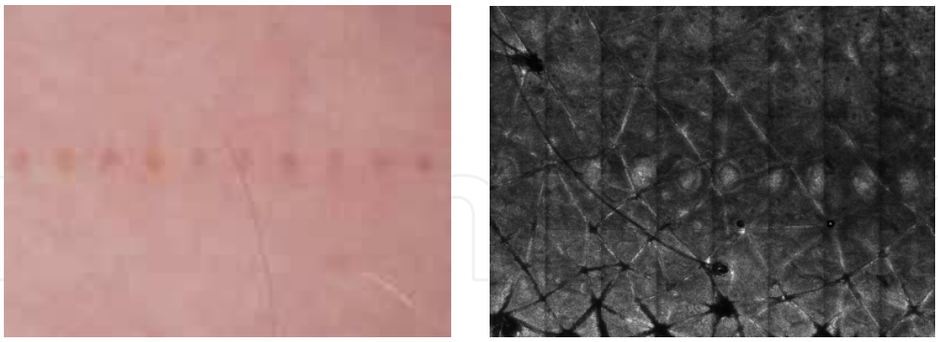

Fig. 9. Corresponding cross-polarized (left) and reflectance CSLM (right) images of a line of micro-wounds created by laser treatment, 1 day post-treatment, are shown. (4 mm x 3 mm)

To monitor the wound healing process of the micro-wounds, three ROIs were defined in each CSLM image stack and their intensity profiles were extracted. The individual treated micro-wound zone (1) and the surrounding collateral damage zone (2) were compared to a normal area away from the micro-wound (3). Their depth-dependent intensity profiles were extracted and analyzed to observe dynamic changes within skin as a response to the micro-wound. The depth-dependent intensity profiles of the 3 ROIs and a series of corresponding

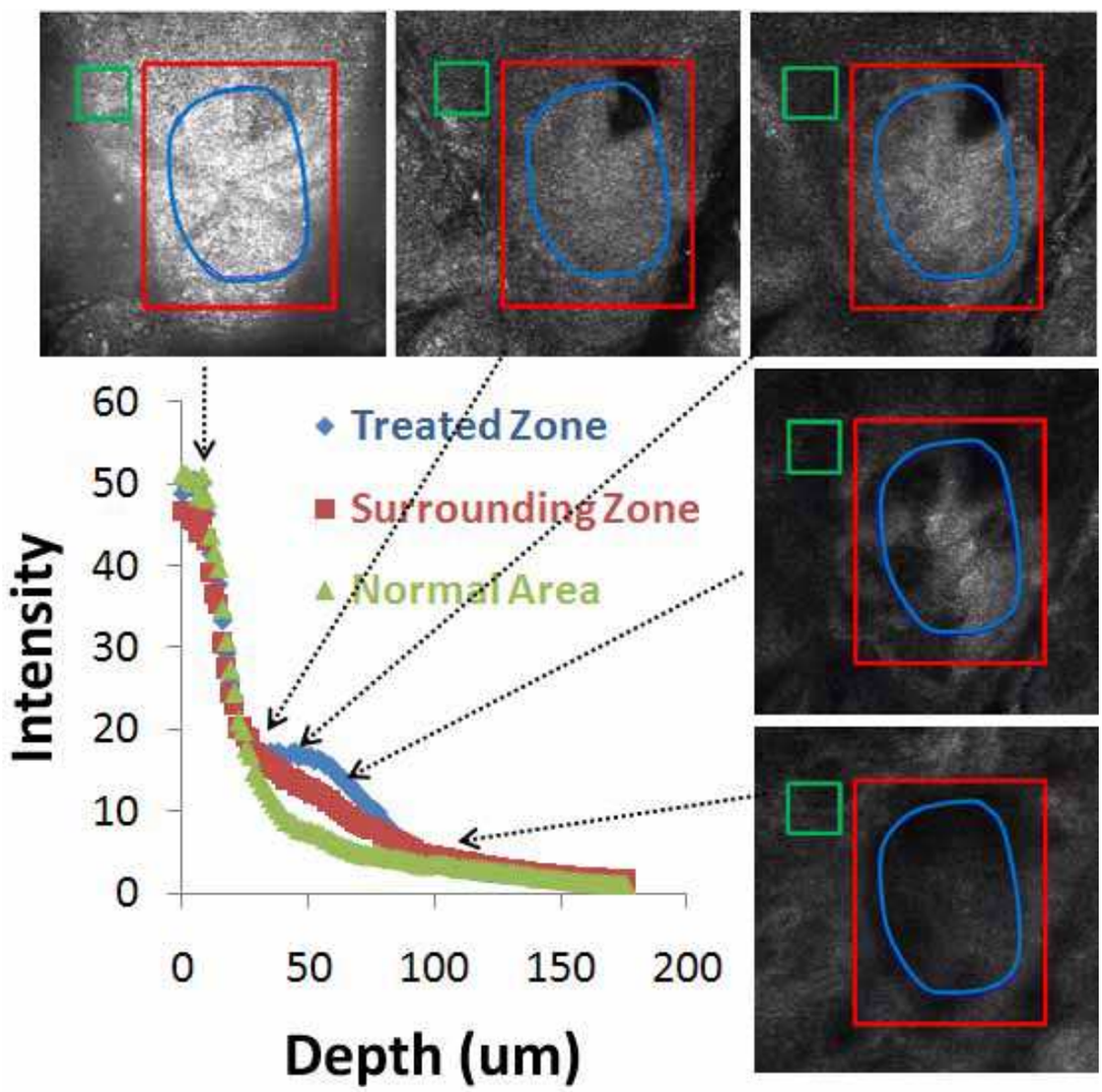

Fig. 10. The depth intensity profiles of the 3 regions are shown, along with confocal images at various depths from a sample image stack, 30 minutes post-treatment.

confocal images at various depths are shown in Figure 10 (data from the volar forearm of a 27 year-old Caucasian female 30 minutes post-treatment). In the confocal images, the region outlined in blue represents the treated micro-wound zone, and the region defined in red, excluding the micro-wound zone (blue region), represents the surrounding area. The normal "control" skin is defined by the green region.

As early as 30 minutes post-treatment, changes in reflectivity are observed in both the micro-wound and the surrounding tissue, indicating cellular changes are occurring both in and around the micro-wound as response to laser treatment. Within the superficial layers, 10-15 μm below the top of the SC, the intensity of reflection in the treated micro-wound zone is only slightly higher compared to the surrounding and normal areas, indicating that there is minimal damage to the surface of the skin. A significant increase in reflection is observed in the micro-wound zone 20-50 μm below the skin surface. This may be due to swelling, causing a mismatch in refractive index from the upper layers. The intensity of reflection slightly decreases within the micro-wound below 50 μm and into the dermis, indicating the dermal collagen may have been denatured from the laser treatment. This may also be due to the tissue becoming optically opaque, so as skin is sectioned deeper, light is lost to scattering and absorption of the tissue.

Dynamic changes of the wound-healing process were observed within the first week and then again 3 weeks after the one-time treatment. Using both CSLM and video microscopy together enables us to identify how changes on the cellular level contribute to what can be seen in magnified images of the skin. Cross-polarized images of the treated site show that micro-wounds are undetectable immediately after treatment, only showing slight edema and inflammation in the images. Within the first 48 hours post-treatment, the micro-wounds appear brown-colored, and as the micro-wounds healed over the 3 weeks, the micro-wounds became invisible (Figure 11).

The depth-dependent intensity profiles provide a quantitative measure of the associated cellular changes captured with CSLM and differentiate the 3 ROIs. Figure 11 also shows representative intensity profiles of the treated micro-wound zone, the surrounding collateral damage zone, and a normal area at various time points, and corresponding confocal images 50 and 120 μm below the surface. Throughout the study, normal skin shows similar intensity profiles, indicating that the treatment had minimal effects outside the treated area. Compared to the normal area, the intensity profiles of the treated micro-wound and the surrounding collateral damage zones show changes in the first 4 days post-treatment and return to profiles similar to normal skin 3 weeks after treatment. Although the surrounding collateral damage zone shows little change from normal skin 30 minutes post-treatment, there is a significant increase in intensity 2 days and 4 days after treatment. The intensity profile of the treated micro-wound, between 20-100 μm below the surface, progressively increases in intensity immediately after treatment until 4 days post-treatment.

To compensate for the intrinsic exponential decay in intensity with increasing depth in CSLM, the intensity profile of the treated micro-wound zone was normalized to the normal "control" area. Figure 12 shows a peak in the normalized intensity profile of the treated zone, and the peak position first shifts deeper before returning to shallower depths as the micro-wound heals. Images at intermediate time points between Days 4 and 21 were also captured for each subject. The transition time when the peak position shifts back to shallower depths appears to depend on age, with the peak of younger subjects shifting back to shallower depths sooner than they do for older subjects. This suggests that younger

individuals heal faster than older individuals, which agrees with clinical observations. This quantitative method can be used to evaluate the wound-healing rate at the cellular level.

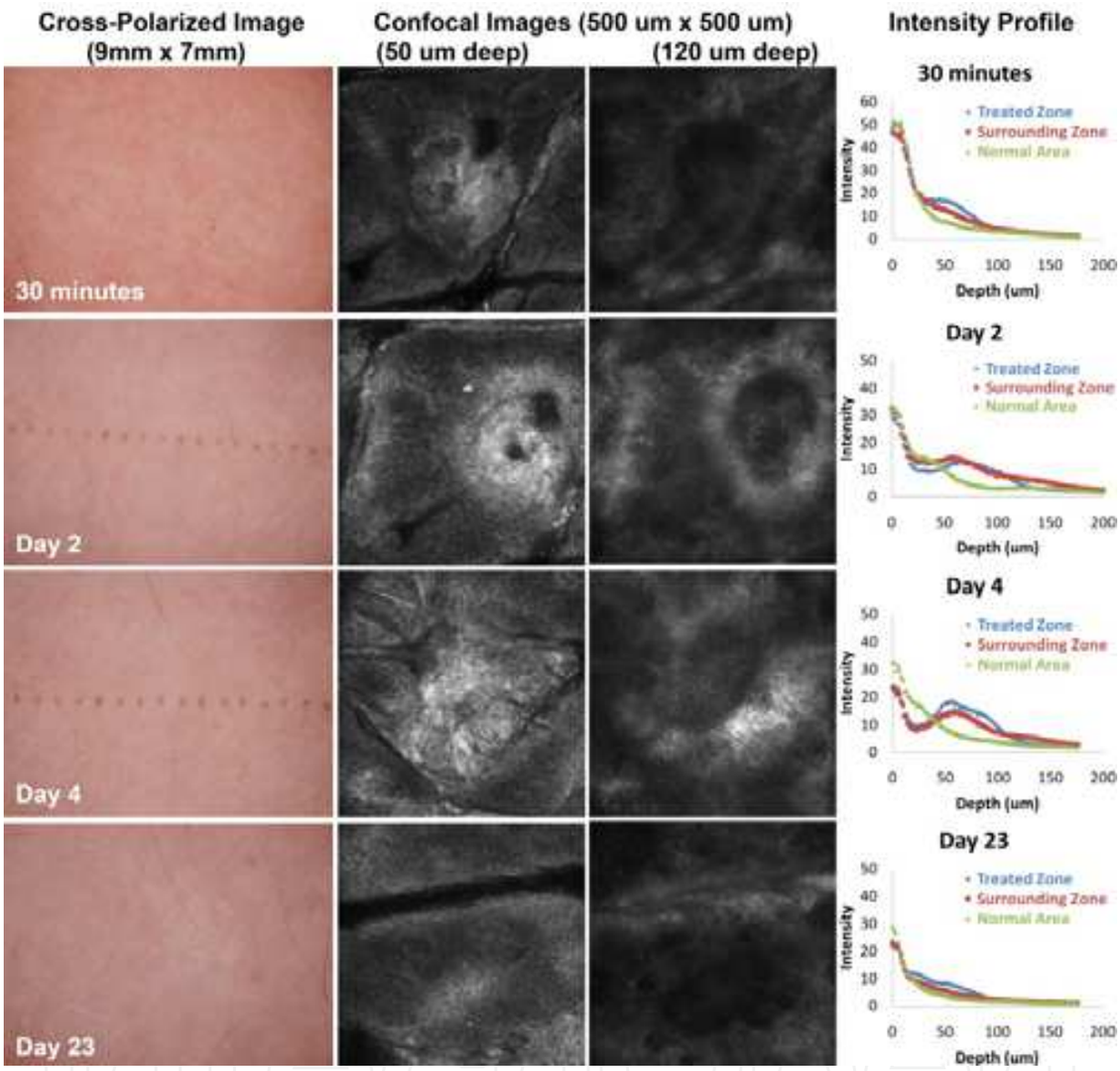

Fig. 11. Representative cross-polarized images of the micro-wounds at various post-treatment time points along with confocal images 50 and 120 µm below the top of the SC. Intensity profiles are also shown.

7. Summary and conclusions

Confocal laser scanning microscopy is a novel technique that enables us to non-invasively investigate skin at the cellular level and dynamic changes that may occur over a period of time. It was shown that the incident light wavelength in CSLM systems affects signal intensity and structural details at the cellular level. Systems equipped with shorter wavelengths may provide improved resolution in images, while those with longer

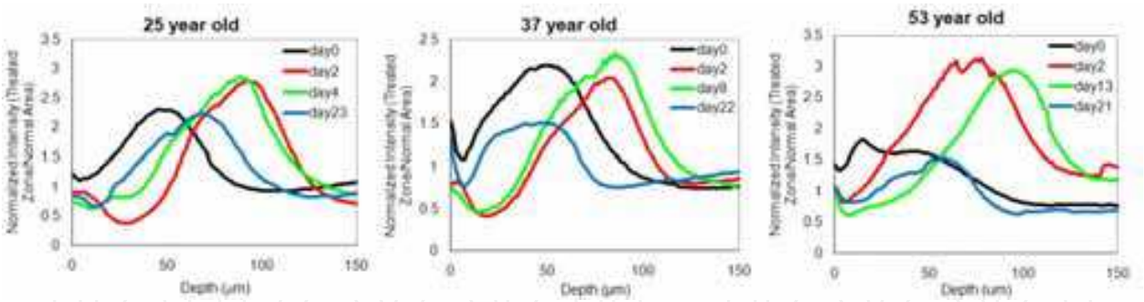

Fig. 12. Normalized intensity profiles within treated zone of 3 subjects at various time points post-treatment.

wavelengths can image deeper into the skin. When comparing systems of the same design and only differing in incident wavelength, the 785 nm system produces images with greater signal intensity and contrast in structural detail compared to the 830 nm system. It is peculiar that imaging human skin with 785 and 830 nm wavelengths produces intensity profiles that appear biphasic, while imaging at 405 nm result in intensity profiles that follow a simple exponential decay. The normalized intensity profiles generated from 405 nm images are also significantly less than those from 785 and 830 nm images at shallow depths.

The studies discussed show the potential of using CSLM to study skin and the cellular processes that occur over time and as a response to wounding. Infant skin is not fully developed and exhibits different characteristics compared to adult skin. With CSLM, we discovered morphological differences between infant and adult skin, which may contribute to the functional differences observed between the developing infant skin and fully-developed adult skin. Future work includes studying how and when infant skin transitions to being adult-like, morphologically. Since we can observe the wound-healing process, we can now evaluate various factors that may affect the wound-healing rate and evaluate how micro-wounds compare to larger skin wounds. We can also evaluate how the method used to create the micro-wound affects the resulting cellular damage.

Capturing cellular changes over time with CSLM is of great significance as it enables us to study the physiology of living skin tissue. Skin is the body's largest functioning organ, consisting of millions of cells that are in constant activity, whether it be proliferation, pigmentation, repair, etc. Capturing the same cells over time and observing their activity is powerful. By studying healthy skin tissue and understanding how it reacts and functions under average conditions, we can better characterize healthy tissue and differentiate between healthy and unhealthy tissue. Capturing physiological and morphological changes in skin due to aging, treatment, and wounding is only the beginning of our fundamental understanding of dynamic cellular changes using CSLM. Having a strong foundation in the knowledge of normal function and activity of healthy tissue is essential to the study and understanding of diseased tissue.

8. Acknowledgements

The authors would like to acknowledge Lucid, Inc. for their use of equipment, confocal microscopy expertise (Zachary M. Eastman) and accessibility to enable the research projects presented within this chapter. A special thanks to Gregory Payonk for the initial version of

the normalized intensity analysis first used in the comparison of mother and infant skin investigation and to Yang Liu who contributed to the improvement of this analysis used in the wound healing response of micro-injuries. The authors would also like to thank Michael Neidrauer for his time and attention spent on data analysis and presentation of the different incident wavelength data.

9. References

Calzavara-Pinton, P., Longo, C., Venturini, M., Sala, R. & Pellacani, G. (2008). Reflectance confocal microscopy for in vivo skin imaging, *Photochemistry and Photobiology* Vol. 84(No. 6): 1421-30.

Gonzalez, S. & Gilaberte-Calzada, Y. (2008). In vivo reflectance-mode confocal microscopy in clinical dermatology and cosmetology, *International Journal of Cosmetic Science* Vol. 30(No. 1): 1-17.

Hantash, B. M. & Mahmood, M. B. (2007). Fractional photothermolysis: a novel aesthetic laser surgery modality, *Dermatologic Surgery* Vol. 33(No. 5): 525-34.

Kollias, N. (1995). The physical basis of skin color and its evaluation, *Clinics in Dermatology* Vol. 13(No. 4): 361-7.

Liu, Y., Bargo, P. & Kollias, N. (2009). Quantitative assessment of wound-healing process as a response to laser-induced micro-injuries, *Proceedings of SPIE*, SPIE, San Jose, California, pp. 71610W1-6.

Luedtke, M. A., Papazoglou, E., Neidrauer, M. & Kollias, N. (2009). Wavelength effects on contrast observed with reflectance in vivo confocal laser scanning microscopy, *Skin Research and Technology* Vol 15(No. 4): 482-8.

Manstein, D., Herron, G. S., Sink, R. K., Tanner, H. & Anderson, R. R. (2004). Fractional photothermolysis: a new concept for cutaneous remodeling using microscopic patterns of thermal injury, *Lasers in Surgery and Medicine* Vol. 34(No. 5): 426-38.

Pellacani, G., Longo, C., Malvehy, J., Puig, S., Carrera, C., Segura, S., Bassoli, S. & Seidenari, S. (2008). In vivo confocal microscopic and histopathologic correlations of dermoscopic features in 202 melanocytic lesions, *Archives of Dermatology* Vol. 144(No. 12): 1597-608.

Rajadhyaksha, M., Grossman, M., Esterowitz, D., Webb, R. H. & Anderson, R. R. (1995). In vivo confocal scanning laser microscopy of human skin: melanin provides strong contrast, *Journal of Investigative Dermatology* Vol. 104(No. 6): 946-52.

Rajadhyaksha, M., Gonzalez, S., Zavislan, J. M., Anderson, R. R. & Webb, R. H. (1999). In vivo confocal scanning laser microscopy of human skin II: advances in instrumentation and comparison with histology, *Journal of Investigative Dermatology* Vol. 113(No. 3): 293-303.

Scope, A., Benvenuto-Andrade, C., Agero, A. L., Malvehy, J., Puig, S., Rajadhyaksha, M., Busam, K. J., Marra, D. E., Torres, A., Propperova, I., Langley, R. G., Marghoob, A. A., Pellacani, G., Seidenari, S., Halpern, A. C. & Gonzalez, S. (2007). In vivo reflectance confocal microscopy imaging of melanocytic skin lesions: consensus terminology glossary and illustrative images, *Journal of American Academy of Dermatology* Vol. 57(No. 4): 644-58.

Stamatas, G. N., Nikolovski, J., Luedtke, M. A., Kollias, N. & Wiegand, B. C. (2009). Infant skin microstructure assessed in vivo differs from adult skin in organization and at the cellular level, *Pediatric Dermatology* Vol. 27(No. 2): 125-31.

Tannous, Z. (2007). Fractional resurfacing, *Clinics in Dermatology* Vol. 25(No. 5): 480-6.

Webb, R. H. (1996). Confocal optical microscopy, *Reports on Progress in Physics* Vol. 59(No. 3): 427-71.

Webb, R. H. (1999). Theoretical basis of confocal microscopy, In: *Methods in Enzymology Volume 307*, P. M. Conn (Ed.), 3-20, Academic Press, ISBN: 978-0-12-182208-8, New York.

Laser Scanning, Theory and Applications
Edited by Prof. Chau-Chang Wang

ISBN 978-953-307-205-0
Hard cover, 566 pages
Publisher InTech
Published online 26, April, 2011
Published in print edition April, 2011

Ever since the invention of laser by Schawlow and Townes in 1958, various innovative ideas of laser-based applications emerge very year. At the same time, scientists and engineers keep on improving laser's power density, size, and cost which patch up the gap between theories and implementations. More importantly, our everyday life is changed and influenced by lasers even though we may not be fully aware of its existence. For example, it is there in cross-continent phone calls, price tag scanning in supermarkets, pointers in the classrooms, printers in the offices, accurate metal cutting in machine shops, etc. In this volume, we focus the recent developments related to laser scanning, a very powerful technique used in features detection and measurement. We invited researchers who do fundamental works in laser scanning theories or apply the principles of laser scanning to tackle problems encountered in medicine, geodesic survey, biology and archaeology. Twenty-eight chapters contributed by authors around the world to constitute this comprehensive book.

InTech Europe
University Campus STeP Ri
Slavka Krautzeka 83/A
51000 Rijeka, Croatia
Phone: +385 (51) 770 447
Fax: +385 (51) 686 166
www.intechopen.com

InTech China
Unit 405, Office Block, Hotel Equatorial Shanghai
No.65, Yan An Road (West), Shanghai, 200040, China
中国上海市延安西路65号上海国际贵都大饭店办公楼405单元
Phone: +86-21-62489820
Fax: +86-21-62489821

IntechOpen